Enhancing the Efficiency of Solution-Processed Polymer:Colloidal Nanocrystal Hybrid Photovoltaic Cells Using Ethanedithiol Treatment

Renjia Zhou,[†] Romain Stalder,[‡] Dongping Xie,[‡] Weiran Cao,[†] Ying Zheng,[†] Yixing Yang,[†] Marc Plaisant,[†] Paul H. Holloway,[†] Kirk S. Schanze,[‡] John R. Reynolds,[‡,§] and Jiangeng Xue[†,*]

[†]Department of Materials Science and Engineering, University of Florida, Gainesville, Florida 32611-6400, United States, [‡]Department of Chemistry, University of Florida, Gainesville, Florida 32611-7200, United States, and [§]School of Chemistry and Biochemistry and School of Materials Science and Engineering, Center for Organic Photonics and Electronics, Georgia Institute of Technology, Atlanta, Georgia 30332-0400, United States

ABSTRACT Advances in colloidal inorganic nanocrystal synthesis and processing have led to the demonstration of organic–inorganic hybrid photovoltaic (PV) cells using low-cost solution processes from blends of conjugated polymer and colloidal nanocrystals. However, the performance of such hybrid PV cells has been limited due to the lack of control at the complex interfaces between the organic and inorganic hybrid active materials. Here we show that the efficiency of hybrid PV devices can be significantly enhanced by engineering the polymer–nanocrystal interface with proper chemical treatment. Using two different conjugated polymers, poly(3-hexylthiophene) (P3HT) and poly[2,6-(4,4-bis(2-ethylhexyl)-4*H*-cyclopenta[2,1-*b*;3,4-*b*′]-dithiophene)-*alt*-4,7-(2,1,3-benzothiadiazole)] (PCPDTBT), we show that treating the polymer:nanocrystal hybrid film in an ethanedithiol-containing acetonitrile solution can increase the efficiency of the hybrid PV devices by 30–90%, and a maximum power conversion efficiency of 5.2 ± 0.3% was obtained in the PCPDTBT:CdSe devices at 0.2 sun (AM 1.5G), which was slightly reduced to 4.7 ± 0.3% at 1 sun. The ethanedithiol treatment did not result in significant changes in the morphology and UV–vis optical absorption of the hybrid thin films; however, infrared absorption, NMR, and X-ray photoelectron spectroscopies revealed the effective removal of organic ligands, especially the charged phosphonic acid ligands, from the CdSe nanorod surface after the treatment, accompanied by the possible monolayer passivation of nanorod surfaces with Cd-thiolates. We attribute the hybrid PV cell efficiency increase upon the ethanedithiol treatment to the reduction in charge and exciton recombination sites on the nanocrystal surface and the simultaneous increase in electron transport through the hybrid film.

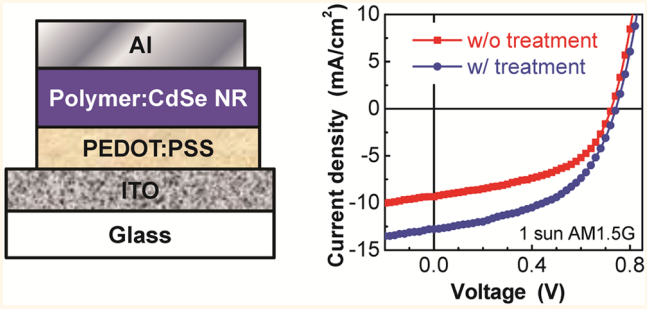

KEYWORDS: polymer:nanocrystal hybrid · photovoltaic cells · interface engineering · colloidal nanocrystals · conjugated polymers

Organic–inorganic hybrid electronic materials have received great interest in recent years due to their applications in various electronic and photonic devices.[1–6] These hybrid materials can potentially combine the low material cost and processing versatility of organic materials with the high carrier mobility and environmental stability of inorganic semiconductors.[1–5] The recent advance in colloidal nanocrystal synthesis has made it possible to process inorganic semiconductors together with organic materials (conjugated polymers and molecules) in solution,[7,8] and the use of such hybrid electronic materials in photovoltaic (PV) cells and light-emitting diodes (LED) is now being explored.[1–3,5,6] Particularly, solution-processed photovoltaic cells using polymer:colloidal nanocrystal hybrids as light-absorbing materials are being considered as a potential type of low-cost solar energy harvesting devices.[1,2,5,9–11]

Since the seminal work on hybrid PV cells based on CdSe nanocrystals and P3HT by Alivisatos and co-workers nearly a decade ago,[1] advances in areas such as nanocrystal synthesis, hybrid material processing, and device structure innovation have increased the power conversion efficiency (η_P) of these devices to above 3%.[5,9–17] The use of nanorods

* Address correspondence to jxue@mse.ufl.edu (J.X.).

Received for review December 17, 2012 and accepted May 13, 2013.

Published online May 13, 2013
10.1021/nn305823w

with large aspect ratio and branched nanocrystals has been demonstrated to be more advantageous compared to spherical nanocrystals due to the existence of directional charge transport paths,[1,9,11] although it has also been shown that the performance of the nanosphere-based hybrid PV cells strongly depends on the size and spatial distribution (especially the existence of percolating paths) of the nanospheres.[15] The use of lower gap polymers such as PCPDTBT also extended the spectral sensitivity of the hybrid PV devices into the near-infrared, leading to $\eta_P > 3\%$.[10,17] Furthermore, the inclusion of a solution-processed ZnO nanoparticle layer between the hybrid active layer and the metal cathode was shown to improve the light harvesting and exciton/charge confinement in the active layer, in addition to significantly prolonging the environmental stability of the hybrid PV cells.[16,17]

However, despite the potential advantages of the hybrid materials, such development significantly lags behind that for all-organic PV cells, in which maximum η_P values exceeding 10% have been reported very recently.[18−24] A critical challenge for polymer:nanocrystal hybrid PV cells lies in the complex hybrid material interface.[25,26] In spite of the superior carrier mobility in bulk inorganic semiconductors, carrier mobilities in colloidal inorganic nanocrystal thin films are typically several orders of magnitude lower, at a level similar to or even lower than those in organic materials, due to the presence of abundant surfaces and complex interfaces involving organic ligands.[15,27] Meanwhile, to facilitate charge transfer between the nanocrystals and polymer, a critical step in the entire photovoltaic process, most of the insulating capping ligands present on nanocrystal surfaces need to be removed; the large number of dangling bonds on the bare nanocrystal surfaces as well as some residual ligands may give rise to a large density of defect states that serve as recombination centers for photogenerated excitons and charge carriers.[28] Hence proper surface passivation of the nanocrystals is needed to prevent the loss of excitons and charge carriers.

Within the past few years, substantial progress[29,30] was also reported for colloidal PbS and PbSe quantum dots based PV cells in which the quantum dots form a neat layer instead of being distributed in a polymer matrix. Different from the polymer:nanocrystal hybrid PV cells in which charge separation occurs at the hybrid material interface, these quantum dot based PV cells rely on a Schottky junction[31] or a junction between the quantum dot layer and another semiconductor (such as ZnO or TiO_2)[32,33] to separate charge carriers upon light absorption. For these PbS- or PbSe-based devices, it has been found that using dithiols to replace the long and insulating oleic acid ligands on the quantum dot surface improves the film-forming characteristics and the hole mobility of the quantum dot film.[34,35] Proper passivation of the quantum dot surface is also shown to be critical for achieving high-efficiency photovoltaic devices.[36]

Here we show that proper treatment of CdSe nanorods in ethanedithiol (EDT) can lead to removal of residual organic ligands on the nanocrystal surface and likely achieve monolayer passivation. This leads to a more favorable interface between the organic and inorganic semiconductors for charge generation and transport. Depending on the polymer used and the CdSe nanorod aspect ratio, we show that this interface engineering approach results in a 30−90% increase in η_P of the hybrid PV cells. Using a low-gap polymer PCPDTBT and high aspect ratio CdSe nanorods, we have achieved a maximum η_P of 4.7 ± 0.3% at 1 sun AM 1.5G solar illumination, which also exceeded 5% at reduced illumination intensities.

RESULTS AND DISCUSSION

The schematic device structure of the polymer:nanocrystal hybrid PV cells is shown in Figure 1a. The transparent conductive indium tin oxide (ITO) layer and Al serve as the anode and cathode, respectively. Both the poly(3,4-ethylenedioxythiophene):poly(styrenesulfonate) (PEDOT:PSS) and the hybrid active layer were spin-coated, resulting in thicknesses of ~40 and ~100 nm, respectively. Here as-synthesized CdSe nanorods[37] were purified and ligand exchanged in pyridine before being blended in chloroform with either poly(3-hexylthiophene) (P3HT) or poly[2,6-(4,4-bis(2-ethylhexyl)-4*H*-cyclopenta[2,1-*b*;3,4-*b*′]-dithiophene)-*alt*-4,7-(2,1,3-benzothiadiazole)] (PCPDTBT) (Figure 1b). After deposition of the hybrid active layer, the samples were immersed in an acetonitrile solution containing 1% ethanedithiol for 1 min (ethanedithiol is a toxic and volatile liquid that should be handled in a nitrogen-filled glovebox; see experimental details in the Supporting Information).

The EDT treatment has previously been demonstrated as an effective approach to shorten the organic surfactants upon lead chalcogenides' quantum dots and enhance the performance of quantum dots based PV cells[38,35] and field-effect transistors.[39] Here this short EDT treatment has a profound impact on the polymer:CdSe hybrid PV device performance. Figure 1c and d compare the current density−voltage ($J-V$) characteristics of representative P3HT:CdSe and PCPDTBT:CdSe hybrid PV cells with and without the EDT treatment, under simulated 1 sun (=100 mW/cm^2) AM 1.5G solar illumination. The CdSe nanorods have an average length of 32 nm and width of 4.4 nm, corresponding to an aspect ratio (AR) of 7 (see Figure S1 in the Supporting Information). It is noted that these hybrid PV devices show unusual aging behavior when exposed to air without encapsulation;[15] the data shown here are for maximum PV performance of these devices after several hours' air exposure (see Supporting Information for more details). The corresponding PV parameters (η_P, short-circuit current density J_{SC}, open-circuit voltage V_{OC}, and fill factor FF) are summarized in Table 1 (for high AR nanorods), which represent statistical

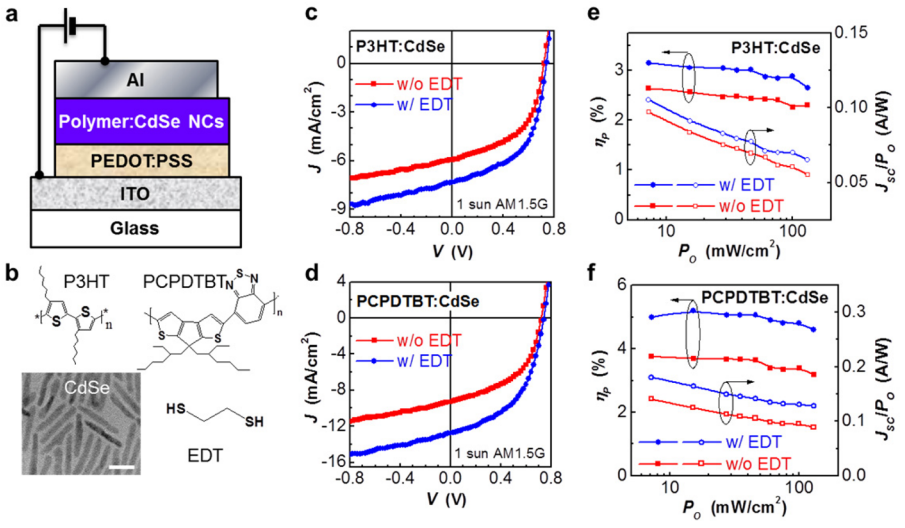

Figure 1. Performance enhancement in polymer:colloidal nanocrystal hybrid PV devices upon EDT treatment. (a) Schematic device structure of polymer:colloidal nanocrystal hybrid PV device. (b) Transmission electron microscopy image of CdSe nanorods (scale bar: 20 nm) and chemical structures of conjugated polymers (P3HT and PCPDTBT) and EDT. The nanorods have an aspect ratio of 7. (c) Current density−voltage (J−V) characteristics of P3HT:CdSe hybrid PV devices with and without EDT treatment. (d) J−V characteristics of PCPDTBT:CdSe hybrid PV devices with and without EDT treatment. (e, f) Illumination power dependence of power conversion efficiency (η_P) and ratio of short-circuit current density (J_{sc}) to P_0 for P3HT:CdSe (d) and PCPDTBT:CdSe (e) hybrid PV devices with and without EDT treatment.

averages over 50 devices for each configuration. The EDT treatment on the P3HT:CdSe devices yields an increase of J_{SC} from 5.9 mA/cm^2 to 7.4 mA/cm^2 (Figure 1c). Together with a slight enhancement in both V_{OC} and FF, the η_P was increased from 2.2 ± 0.2% to 2.9 ± 0.2% after the EDT treatment, a relative enhancement of approximately 30% (Table 1).

The efficiency of hybrid PV cells can be enhanced by using the narrow-gap polymer PCPDTBT to effectively harvest infrared photons.[10,17,40] As shown in Figure 1d and Table 1, the PCPDTBT:CdSe cell yields a η_P of 3.3% under 1 sun illumination. When the active layer was treated with EDT, a substantial increase in J_{SC} from 9.3 mA/cm^2 to 12.8 mA/cm^2 was observed, which, accompanied with slight increases in both V_{OC} and FF, leads to η_P = 4.7 ± 0.3% under 1 sun illumination, representing an approximately 40% relative increase.

We further characterized the performance of these devices under variable illumination intensities (P_0). As shown in Figure 1e and f, for both representative P3HT:CdSe and PCPDTBT:CdSe devices with and without the EDT treatment, the ratio of J_{SC} to P_0, which corresponds to the external quantum efficiency, decreases as P_0 increases from 0.07 sun to 1.3 sun. This behavior suggests the presence of strong bimolecular recombination within the active layers,[41] which becomes more serious in active layer with low charge carrier mobilities at higher P_0 due to the higher photogenerated carrier concentrations. Partly offset by the increase of V_{OC} with P_0,[42] this leads to η_P of the devices peaking at low intensities (P_0 < 0.2 sun). Nevertheless, the EDT treatment leads to a ~15% and ~35% increase in J_{SC}/P_0 for the P3HT- and PCPDTBT-based devices, respectively, across the entire P_0 range. The maximum η_P for the P3HT:CdSe devices was increased from 2.6 ± 0.2% to 3.2 ± 0.2% upon the EDT treatment, whereas it was increased from 3.7 ± 0.2% to 5.2 ± 0.3% for the PCPDTBT:CdSe devices.

TABLE 1. Summary of Photovoltaic Performance under 1 sun AM 1.5 G Illumination for Polymer:Colloidal Nanocrystal Hybrid Photovoltaic Cells

polymer	CdSe NRs	EDT treatment	J_{SC} (mA/cm^2)	V_{OC} (V)	FF	η_P (%)	$\Delta\eta_P/\eta_P$ (%)
P3HT	low AR[a]	no	4.9	0.73	0.39	1.4 ± 0.1	
		yes	7.1	0.71	0.51	2.6 ± 0.2	86
PCPDTBT	low AR[a]	no	6.6	0.72	0.39	1.9 ± 0.1	
		yes	9.9	0.72	0.46	3.3 ± 0.2	74
P3HT	high AR[b]	no	5.9	0.72	0.52	2.2 ± 0.2	
		yes	7.4	0.73	0.54	2.9 ± 0.2	32
PCPDTBT	high AR[b]	no	9.3	0.72	0.49	3.3 ± 0.2	
		yes	12.8	0.74	0.50	4.7 ± 0.3	42

[a] Low AR = 2 (length: 14 nm, width: 6.4 nm). [b] High AR = 7 (length: 32 nm, width: 4.4 nm).

The external quantum efficiency (EQE) spectra of these devices are shown in Figure 2a. The P3HT:CdSe hybrid PV device shows higher EQE at wavelengths from λ = 350 to 550 nm with EDT treatment, and a maximum EQE of 54% was achieved at λ = 375 nm. Meanwhile, the device based on PCPDTBT shows a broader photoresponse range from λ = 300 to 850 nm due to the lower optical gap of PCPDTBT (1.45 eV)[40] than that of P3HT (1.9 eV).[43] The EDT treatment leads to higher EQE over the entire photoresponsive spectral range for the PCPDTBT:CdSe device, particularly at λ < 750 nm. The absorption spectra of the P3HT:CdSe and PCPDTBT:CdSe hybrid films, however, are nearly

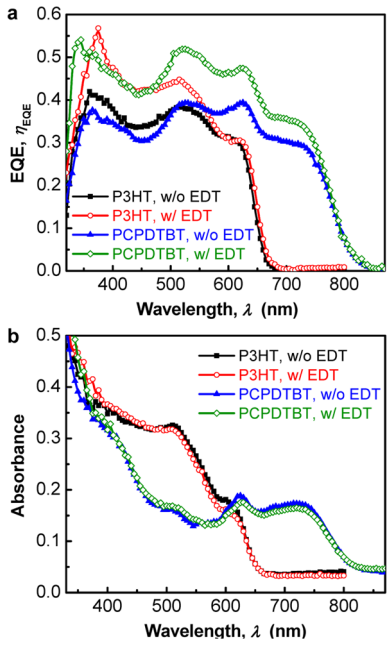

Figure 2. Spectral sensitivity of polymer:colloidal nanocrystal hybrid PV cells. (a) External quantum efficiency (EQE) of hybrid polymer:colloidal nanocrystal PV devices. (b) Absorbance of polymer:colloidal nanocrystal hybrid films deposited on glass.

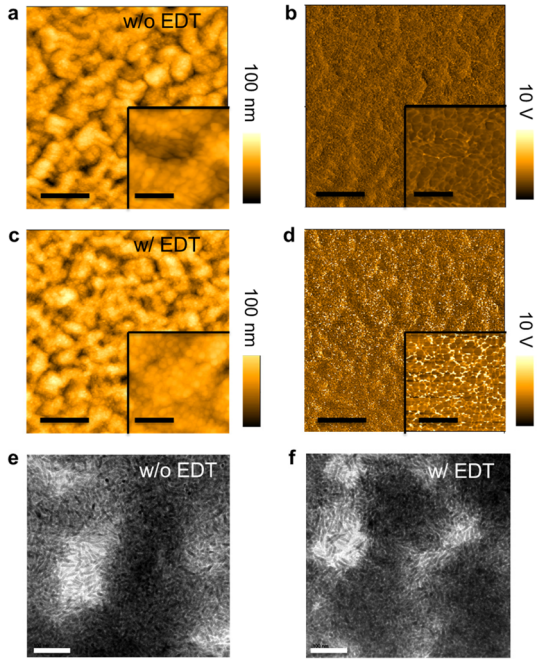

Figure 3. Morphologies of PCPDTBT:colloidal nanocrystal hybrid. (a, b,) Tapping mode atomic force microscopy (AFM) topographies and their corresponding phase images of PCPDTBT:CdSe NR hybrid films without EDT treatment (scale bar: 1 μm). (c, d) Tapping mode AFM topographies and their corresponding phase images of PCPDTBT:CdSe NR hybrid films with EDT treatment (scale bar: 1 μm). Inset: Close-up topographical image and the corresponding phase images (scale bar: 200 nm). (e, f) Transmission electron micrographs of P3HT:CdSe NR hybrid films without and with EDT treatment (scale bar: 100 nm).

identical before and after EDT treatment (Figure 2b). This suggests that the EDT treatment does not result in changes in the bulk properties of the active layer, such as material gain/loss or structural ordering, and any potential changes are likely concerned with the interfaces between the materials.

It was also observed that the performance of hybrid PV devices also has strong dependencies on the length and aspect ratio of the CdSe nanorods. When nanorods with a length of 14 nm and width of 6.4 nm (AR $\approx$ 2, see Figures S1 and S5 in the Supporting Information) were used, as already summarized in Table 1, the hybrid PV devices show significantly lower performance (η_P = 1.4% for P3HT-based and η_P = 1.9% for PCPDTBT-based devices) than similar ones with higher AR nanorods. However, when treated with EDT, these devices exhibit a more substantial improvement in J_{SC} (45% for P3HT-based and 50% for PCPDTBT-based devices). Along with a significant increase in the FF (from 0.39 to 0.51 or 0.46), this leads to ~80% enhancement in η_P for the two devices, significantly higher than the 30−40% enhancement for those with higher AR nanorods.

To understand the nature of the EDT treatment on the hybrid materials and its impact on PV device performance, we have carried out a series of structural, chemical, and electronic characterization on the hybrid materials. Figure 3 shows the atomic force microscopy (AFM) morphology and phase images of the PCPDTBT:CdSe hybrid film before and after EDT treatment. Without the EDT treatment, large domains with size of 200−600 nm are observed (Figure 3a). As suggested by the uniform phase image (Figure 3b), these large domains do not correspond to either pure polymer or pure nanocrystal domains. The close-up images shown in the insets reveal that each large domain consists of many smaller domains with a size of 30−50 nm. Upon EDT treatment, the hybrid layer shows no noticeable change in the surface topology and the root-mean-square surface roughness remains at $R_{rms} \approx 10$ nm. The phase image (Figure 3d) shows an enhanced contrast for some regions among the small domains, suggesting a more rigid surface after the EDT treatment. Further morphological characterization by transmission electron microscopy (TEM) of the P3HT:CdSe NR films, as shown in Figure 3e and f, also indicates there is no noticeable change for the hybrid films without and with the EDT treatment (also see Supporting Information, Figure S2).

The EDT treatment does have a more profound impact on the surface chemistry of CdSe nanocrystals. During synthesis, organic surfactants including trioctylphosphonine oxide (TOPO) and tetradecylphosphonic acid (TDPA) were involved (Supporting Information), which were attached to the nanocrystal surface to stabilize nanocrystals after synthesis.[8,44] Figure 4a shows the Fourier transform infrared (FTIR) transmittance spectra of CdSe nanorods that are purified after synthesis, ligand

exchanged in pyridine, and after EDT treatment. The absorption peaks at 2921 and 2847 cm^{-1} are due to the C−H stretching vibration in $-CH_3$ groups from either TOPO or TDPA. The intensities of these absorption peaks are decreased after ligand exchange in pyridine and nearly vanish after EDT treatment, suggesting that the alkyl-based organic ligands can be effectively removed by ligand exchange with pyridine and by EDT treatment. Moreover, the presence of the absorption peaks at 1098 and 931 cm^{-1}, which correspond to stretching vibrations of P═O and P−O, respectively, suggests the abundance of TOPO and TDPA (which contains both P═O and P−O) on the nanocrystal surface.[45] The P═O and P−O peak intensities are reduced by approximately 70% and 55%, respectively, after pyridine exchange; however these peaks are nearly completely suppressed after EDT treatment (also see Supporting Information, Figure S3). This suggests that these phosphorus-based ligands are only partially removed after ligand exchange with pyridine; however, the EDT treatment is effective in completely removing these phosphorus-based surfactants.

The cleavage processes of organic ligands adsorbed on the CdSe surface have been further investigated by phosphorus nuclear magnetic resonance spectroscopy (^{31}P NMR). The purified CdSe nanorods dispersed in deuterochloroform ($CDCl_3$) with a concentration of ~50 mg/mL do not show any distinct signal in the ^{31}P NMR. This behavior may be explained by the fact that the nanorod concentration (or the phosphorus-containing ligands' concentration) is insufficient or the signals of the surface-bound ligands are broadened due to the slow rotational correlation time of the nanorods. However, as shown in Figure 4b, after the ligand-exchange reaction in pyridine, the exchanged ligands contained in the supernatant (collected after precipitating nanorods) exhibit a peak at 50.8 ppm, which is due to the free TOPO.[46−49] Pyridine-exchanged nanorods in $CDCl_3$ have been further treated by EDT with a small amount of triethylamine (TEA) as a Lewis base.[44] The NMR spectrum of the resulting supernatant exhibits three sharp peaks located at 26.7, 21.5, and 18.7 ppm, respectively. The peaks at 26.7 and 18.7 ppm can be assigned to the phosphorus in TDPA and *P*,*P*′-(di-*n*-tetradecyl) dihydrogen pyrophosphonic acid (PPA, created by the condensation of two TDPA molecules at high temperature), respectively,[46−49] while the peak at 21.5 ppm may be due to the formation of a TDPA-TEA salt or other unknown phosphonic acid (PA) species. Hence, this study shows that pyridine exchange is effective in removing the neutral, or "L-type", TOPO ligand, whereas the charged, or "X-type", phosphonic acid ligands (TDPA and PPA), which have higher bonding affinity to the CdSe nanocrystals, can be removed only after the EDT treatment. Combining FTIR and NMR results and integrating the absorption peaks for the methyl group at 2921 and 2847 cm^{-1} in the FTIR spectra,[45] we estimate that, according to the Lambert−Beer law, 65 ± 10% of the organic ligands (primarily TOPO) are removed after ligand exchange with pyridine and 90 ± 10% of the total ligands can be eliminated after EDT treatment following pyridine ligand exchange (see Supporting Information, Figure S3).

Although FTIR and NMR give a clear picture that surface ligands on the nanocrystals can be removed step-by-step by pyridine exchange and by EDT treatment, the detailed cleavage processes and the chemical bonding nature are still unclear. Here X-ray photoelectron spectroscopy (XPS) was employed to further probe the chemical states of various elements. Figure 4c shows the C 1s XPS spectra for nanorods processed using various conditions. The intensity of the C 1s peak is reduced approximately by one-half after ligand exchange in pyridine. With additional EDT treatment but without annealing, a slight increase in the C 1s intensity was observed, which may be attributed to the absorption of EDT molecules to the CdSe nanocrystal surface. Thermal annealing of the EDT-treated sample leads to a sharp reduction in the C 1s peak intensity, suggesting the successful removal of most organic ligands from the nanocrystal surface. The P 2p spectra shown in Figure 4d appear to indicate a chemical shift of 0.5 to 0.8 eV between the purified, pyridine-exchanged, and EDT-treated (without annealing) nanocrystal samples, although the low signal level and broad spectral distribution make the result somewhat difficult to define. The results are more conclusive for the EDT-treated sample after thermal annealing, where the XPS spectrum clearly shows the disappearance of P in the film. These XPS results therefore suggest that the EDT treatment process first results in the release of the phosphonic acids (TDPA and PPA) from the nanocrystal surface, which are then removed from the films following thermal annealing.

For the EDT-treated and annealed sample, we have also attempted to probe the presence of S in the film. This is challenging, as the binding energies of the S 2s and 2p states overlap with those of the Se 3s and 3p states, respectively. Nevertheless, as shown in Figure 4e and f, in addition to the Se peaks at 160.0 eV (Se $3p_{3/2}$), 165.5 eV (Se $3p_{1/2}$), and 229.0 eV (Se 3s), which match well with the published XPS data for CdSe,[50] we can also identify peaks at 162.1, 163.8, and 227.1 eV, which correspond to S $2p_{3/2}$, $2p_{1/2}$, and 2s states, respectively. The surface S to Se ratio is estimated to be 30 ± 10% according to the individual peak intensities. The binding energies of the S 2s and S $2p_{3/2}$ states are 0.5 to 1 eV higher than the reported values for CdS but are ~1 eV lower than those for thiols. They are, however, in agreement with those for ethanedithiolate.[35] Hence, we conclude that the chemical nature of S present in this EDT-treated sample is of Cd-thiolate, rather than either CdS or EDT.

For the colloidal nanocrystals synthesized with both L-type ligands (neutral molecules such as TOPO) and

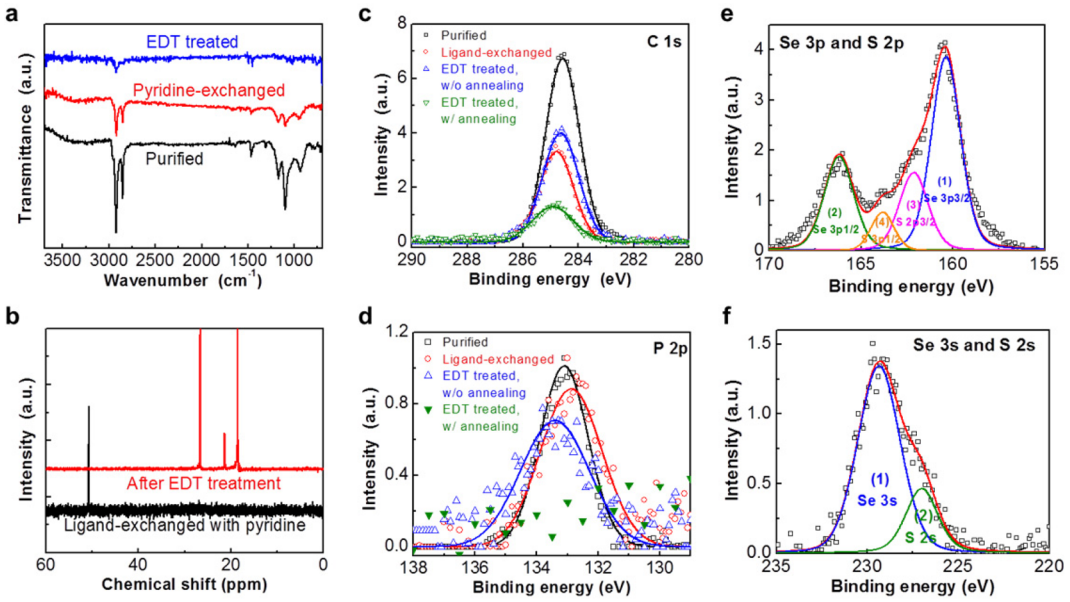

Figure 4. Surface chemistry of colloidal nanocrystals upon EDT treatment. (a) Fourier transform infrared spectra of CdSe nanorods purified after synthesis (black curve), ligand exchanged with pyridine (red curve), and treated with EDT (blue curve). (b) ^{31}P NMR spectra of ligands exchanged by pyridine (black curve) and ligands exchanged by EDT (red curve) from nanorods. (c, d, e, f) XPS high-resolution spectra for C 1s (c), P 2p (d), Se 3p and S 2p (e), and Se 3s and S 2s (f).

X-type ligands (charged molecules such as TDPA), the nanocrystals have a composition of a CdSe core, a monolayer of Cd^{2+} shell, and a monolayer of mixed L-type (TOPO) and X-type ligands (phosphonic acids) (see Supporting Information, Figure S6).[44,48] The L-type ligand bonds to the CdSe surface through weak van der Waals interaction, while the X-type ligand bonds to Cd^{2+} through much stronger Coulombic interactions.[44,48] Particularly, an X-type ligand with a single phosphonic acid group such as TDPA preferentially bonds to Cd cations as a monodentate hydrogen phosphonate, while PPA with two phosphonic acid groups tends to bond Cd cations as bidentate hydrogen phosphonates. The ligand-exchange interaction in pyridine, as revealed by ^{31}P NMR, removes only the L-type ligands. On the basis of the above ^{31}P NMR and XPS results and the detailed study on the surface chemistry of CdSe nanocrystals by several other groups,[44,45,47,48] we propose the following cleavage mechanism of X-type ligands (phosphonic acid species) from the CdSe surface upon EDT treatment. A free EDT molecule adsorbs to the CdSe surface and bonds weakly with a Cd cation, which also weakens the S−H bond in EDT. In a concerted process with the assistance of a Lewis base acetonitrile (also used as the solvent),[31] the adsorbed phosphonic acid ligand leaves the Cd while serving to deprotonate the nearby adsorbed thiol (R−SH) moiety, which also leads to the eventual formation of Cd-thiolate. The overall reaction is illustrated in Figure 5b, while the possible step-by-step reactions are provided in the Supporting Information (Scheme S1).

The charged X-type PA ligands on the nanocrystal surface are expected to form defect states that act as charge-trapping centers and charge/exciton recombination

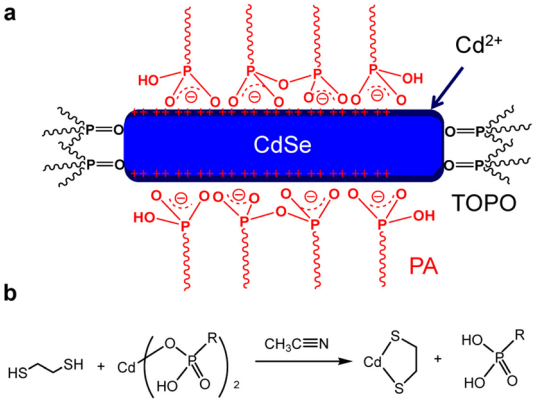

Figure 5. Proposed cleavage mechanism of phosphonic acids (X-type ligands) upon EDT treatment. (a) Schematic illustration of surface chemistry of colloidally synthesized CdSe nanorods. TOPO: trioctylphosphine oxide, PA: phosphonic acid. (b) Proposed cleavage mechanism of PA molecules from nanocrystals upon EDT treatment.

centers.[36,38] Removal of these X-type ligands and simultaneous formation of Cd-thiolate upon EDT treatment lead to the reduction of defect state density and monolayer passivation of the nanocrystal surface. This certainly is beneficial to reduce exciton and charge recombination loss at the organic−inorganic hybrid interface, thereby leading to a higher J_{SC} in the corresponding PV cells. An early study in PbS quantum dot solar cells also indicated that the EDT treatment mainly results in the reduction of the loss in nonradiative exciton recombination.[38] In addition, the reduction of defect states should also increase electron transport through the hybrid film. This is confirmed by the measured electron mobility increase from $\mu_e = 3 \times 10^{-6}$ to

6×10^{-5} cm^2/V·s for the PCPDTBT:CdSe film after the EDT treatment. It is also likely that the removal of the bulky PA ligands also improves the electronic wave overlap between adjacent nanocrystals, thus contributing to the improved electron mobility. The hole mobility, on the other hand, remains at $\mu_h = 1 \times 10^{-5}$ cm^2/V·s after the EDT treatment, suggesting the impact of EDT treatment is mostly on the nanocrystals. The increase in electron mobility thus leads to more favorable collection of photogenerated electrons, also in agreement with the slight enhancement in FF for devices with EDT treatment.

The improvement in charge transport after EDT treatment further explains the higher level of performance increase for the devices with shorter NRs. Due to the shorter NRs, those devices are more prone to charge trapping, which leads to lower overall η_P for the hybrid film and lower FF and J_{SC} from the corresponding hybrid PV cells. Hence removal of charge recombination centers upon EDT treatment has an even stronger impact on enhancing device performance.

CONCLUSIONS

We have demonstrated that the AM 1.5G power conversion efficiency of polymer:colloidal nanocrystal PV cells can be significantly enhanced *via* interface engineering and has reached 4.7% under 1 sun illumination and over 5% under 0.1−0.5 sun illumination for the PCPDTBT:CdSe hybrid devices in this work. The EDT treatment results in removal of charged surface ligands and formation of Cd-thialate on CdSe nanocrystal surfaces. We attribute this effect to the passivation of surface defects on CdSe nanocrystals, which leads to reduced exciton and charge carrier recombination and increased electron transport. Further improvement in the efficiency of such solution-processed polymer:colloidal nanocrystal hybrid PV cells may rely on deeper understanding and better control of the chemistry and physics of the colloidal nanocrystal surface/interface.[51,52] It may also require specially tailored polymers and nanocrystals to achieve better solar spectrum coverage and more optimal energy level alignment, as well as employing advanced device architectures such as tandem cells,[19,53] to make such hybrid PV devices a truly low-cost energy-harvesting technology. The unusual positive aging behavior of these devices upon a few hours of air exposure also needs to be further studied to understand its origin, which could have a strong impact in eventually achieving good environmental and operational stability.

METHODS

CdSe Nanorod Processing and Polymer:CdSe Hybrid Solution Preparation. CdSe nanorods were synthesized according to the reported procedure (details given in the Supporting Information).[37] All nanorods were purified by dissolving into toluene and precipitated with methanol six times. After purification, nanorods were ligand exchanged in pyridine. Then ~80 mg of CdSe nanorods was mixed with 15 mL of pyridine and refluxed for 24 h under N_2 flow. The nanorods were recovered by precipitation with hexane and centrifugation. Polymer:CdSe nanorod hybrids were prepared by dispersing 30 mg of CdSe nanorods into 1 mL of chloroform followed by mixing with 3.0 mg of P3HT or PCPDTBT, resulting in a 10:1 nanocrystal to polymer weight ratio. P3HT (Rieke Metals, molecular weight ~50−70 kg/mol) and PCPDTBT (Luminescence Technology Corp., molecular weight ~8 kg/mol) were used as purchased.

Polymer:Colloidal Nanocrystal Hybrid PV Device Fabrication and Measurement. Polymer:CdSe hybrid PV devices were fabricated as follows. Patterned ITO-coated glass was cleaned with soap, deionized water, acetone, and 2-propanol, respectively, and then was treated in UV-ozone for 15 min. A layer of PEDOT:PSS (~40 nm thick) was spin-coated on ITO and annealed for 15 min at 150 °C in air. The polymer:CdSe hybrid film (~100 nm thick) was spin-coated on PEDOT:PSS in a N_2 glovebox. For devices with EDT treatment, the spin-coated hybrid film was immersed into an acetonitrile solution containing 1% EDT for 1 min and then rinsed in pure acetonitrile. The active layer was annealed at 120 °C for 20 min in the glovebox. The devices were completed by vacuum deposition of an Al cathode (100 nm thick) in a custom high-vacuum chamber (background pressure ~1×10^{-6} Torr). The active PV device area is 4 mm^2 as defined by the patterned electrodes in a cross-bar geometry.

Current−voltage characteristics of these hybrid PV devices in the dark and under simulated AM 1.5G 1 sun illumination from a Xe-arc lamp were measured in laboratory ambient with encapsulation using an Agilent 4155C semiconductor parameter analyzer. Typically a few hours of air exposure leads to maximal device performance[14] (see Supporting Information). The light intensity from the solar simulator was determined using a calibrated single-crystalline silicon reference cell with a KG1 filter, and the spectral mismatch factor was corrected according to the ASTM standard E973. The mismatch factor (M) is 0.99 for all P3HT:CdSe hybrid PV devices and 0.98 for all PCPDTBT:CdSe hybrid PV devices. To measure the external quantum efficiency, the white light emission from the Xe-arc lamp was shone through an Oriel monochromator, and the monochromatic light was chopped at 400 Hz by a mechanical chopper prior to incident onto the device. The devices were illuminated by a constant white light bias from a halogen lamp with an intensity of approximately 100 mW/cm^2 in order to set up the electric field and charge carrier distribution as specified by the ASTM E1021 standard.[54] The photocurrent was measured using a Stanford Research Systems 830DSP lock-in amplifier and Keithley 428 current amplifier. The monochromatic light intensity was measured using a calibrated Newport 818-UV Si detector. The measured EQE spectra were integrated with the standard 1 sun AM 1.5 G solar spectrum, and we verify that the calculated J_{SC} value indeed agrees with the experimental result within experimental error. Efficiency and other performance data reported here represent averages over 50 devices for each device structure, which generally show 5−10% variations.

Single Carrier Device Fabrication and Measurement. For hole-only device fabrication, all the procedures are the same as the PV device fabrication, with the only exception of depositing 100 nm thick gold instead of Al as the top electrode. For electron-only device fabrication, vacuum-deposited Al was used for both bottom and top electrodes sandwiching the hybrid active layer. Both the hole-only and electron-only devices were tested in the dark. The active layer in both hole-only and electron-only devices is 100 nm, as calibrated by both AFM and profilometer measurement. The hole and electron mobilities are obtained by fitting $J-V$ curves according to Child's law:[55] $J = (9/8)\varepsilon_r \times \varepsilon_0 \times \mu \times (V^2/L^3)$, where ε_r is the average of dielectric constant of hybrid film (6.5), ε_0 the permittivity of the free space, μ the hole or electron mobility, L the thickness of the active layer (~100 nm), and V the voltage applied.

Characterization. FTIR spectra were collected with Perkin FTIR spectroscopy by depositing CdSe nanorods on a sodium

chloride substrate. ^{31}P NMR spectra were recorded on a Varian VXR 300 spectrometer (300 MHz). XPS data were collected on a PHI 6100 X-ray photoelectron spectrometer using a magnesium anode with a step size of 0.1 eV. AFM measurement was performed on the devices with a Veeco Innova scanning probe microscope operating in tapping mode.

Conflict of Interest: The authors declare no competing financial interest.

Supporting Information Available: Experimental details on CdSe nanorods synthesis, processing, and characterization, and hybrid film processing and characterization. Hybrid PV device fabrication and measurement. Proposed chemical reaction of CdSe nanocrystals with EDT treatment. This material is available free of charge *via* the Internet at http://pubs.acs.org.

Acknowledgment. The Major Analytical Instrumentation Center (MAIC) at the University of Florida is gratefully acknowledged for measurement assistance.

REFERENCES AND NOTES

1. Huynh, W. U.; Dittmer, J. J.; Alivisatos, A. P. Hybrid Nanorod-Polymer Solar Cells. *Science* **2002**, *295*, 2425–2427.
2. McDonald, S. A.; Konstantatos, G.; Zhang, S.; Cyr, P. W.; Klem, E. J. D.; Levina, L.; Sargent, E. H. Solution-Processed PbS Quantum Dot Infrared Photodetectors and Photovoltaics. *Nat. Mater.* **2005**, *4*, 138–142.
3. Colvin, V. L.; Schlamp, M. C.; Alivisatos, A. P. Light-Emitting-Diodes Made from Cadmium Selenide Nanocrystals and a Semiconducting Polymer. *Nature* **1994**, *370*, 354–357.
4. Kagan, C. R.; Mitzi, D. B.; Dimitrakopoulos, C. D. Organic-Inorganic Hybrid Materials as Semiconducting Channels in Thin-Film Field-Effect Transistors. *Science* **1999**, *286*, 945–947.
5. Oosterhout, S. D.; Wienk, M. M.; van Bavel, S. S.; Thiedmann, R.; Koster, L. J. A.; Gilot, J.; Loos, J.; Schmidt, V.; Janssen, R. A. J. The Effect of Three-Dimensional Morphology on the Efficiency of Hybrid Polymer Solar Cells. *Nat. Mater.* **2009**, *8*, 818–824.
6. Qian, L.; Zheng, Y.; Xue, J.; Holloway, P. H. Stable and Efficient Quantum-Dot Light-Emitting Diodes Based on Solution-Processed Multilayer Structures. *Nat. Photon.* **2011**, *5*, 543–548.
7. Peng, X.; Manna, L.; Yang, W.; Wickham, J.; Scher, E.; Kadavanich, A.; Alivisatos, A. P. Shape Control of CdSe Nanocrystals. *Nature* **2000**, *404*, 59–61.
8. Yin, Y.; Alivisatos, A. P. Colloidal Nanocrystal Synthesis and the Organic-Inorganic Interface. *Nature* **2005**, *437*, 664–670.
9. Sun, B.; Marx, E.; Greenham, N. C. Photovoltaic Devices Using Blends of Branched CdSe Nanoparticles and Conjugated Polymers. *Nano Lett.* **2003**, *3*, 961–963.
10. Dayal, S.; Kopidakis, N.; Olson, D. C.; Ginley, D. S.; Rumbles, G. Photovoltaic Devices with a Low Band Gap Polymer and CdSe Nanostructures Exceeding 3% Efficiency. *Nano Lett.* **2010**, *10*, 239–242.
11. Zhou, R.; Xue, J. Hybrid Polymer-Nanocrystal Materials for Photovoltaic Applications. *ChemPhysChem* **2012**, *13*, 2471–2480.
12. Sun, B.; Snaith, H. J.; Dhoot, A. S.; Westenhoff, S.; Greenham, N. C. Vertically Segregated Hybrid Blends for Photovoltaic Devices with Improved Efficiency. *J. Appl. Phys.* **2005**, *97*, 014914.
13. Sun, B.; Greenham, N. C. Improved Effciency of Photovoltaics Based on CdSe Nanorods and Poly(3-hexylthiophene) Nanofibers. *Phys. Chem. Chem. Phys.* **2006**, *8*, 3557–3560.
14. Gur, I.; Fromer, N. A.; Chen, C. P.; Kanaras, A. G.; Alivisatos, A. P. Hybrid Solar Cells with Prescribed Nanoscale Morphologies Based on Hyperbranched Semiconductor Nanocrystals. *Nano Lett.* **2007**, *7*, 409–414.
15. Yang, J.; Tang, A.; Zhou, R.; Xue, J. Effects of Nanocrystal Size and Device Aging on Performance of Hybrid Poly(3-hexylthiophene):CdSe Nanocrystal Solar Cells. *Sol. Energy Mater. Sol. Cells* **2011**, *95*, 476–482.
16. Qian, L.; Yang, J.; Zhou, R.; Tang, A.; Zheng, Y.; Tseng, T.-K.; Bera, D.; Xue, J.; Holloway, P. H. Hybrid Polymer-CdSe Solar Cells with a ZnO Nanoparticle Buffer Layer for Improved Efficiency and Lifetime. *J. Mater. Chem.* **2011**, *21*, 3814–3817.
17. Zhou, R.; Zheng, Y.; Qian, L.; Yang, Y.; Holloway, P. H.; Xue, J. Solution-Processed, Nanostructured Hybrid Solar Cells with Broad Spectral Sensitivity and Stability. *Nanoscale* **2012**, *4*, 3507–3514.
18. Li, G.; Shrotriya, V.; Huang, J.; Yao, Y.; Moriarty, T.; Emery, K.; Yang, Y. High-Efficiency Solution Processable Polymer Photovoltaic Cells by Self-Organization of Polymer Blends. *Nat. Mater.* **2005**, *4*, 864–868.
19. Kim, J. Y.; Lee, K.; Coates, N. E.; Moses, D.; Nguyen, T. Q.; Dante, M.; Heeger, A. J. Efficient Tandem Polymer Solar Cells Fabricated by All-Solution Processing. *Science* **2007**, *317*, 222–225.
20. Park, S. H.; Roy, A.; Beaupre, S.; Cho, S.; Coates, N.; Moon, J. S.; Moses, D.; Leclerc, M.; Lee, K.; Heeger, A. J. Bulk Heterojunction Solar Cells with Internal Quantum Efficiency Approaching 100%. *Nat. Photon.* **2009**, *3*, 297–303.
21. Xue, J. Perspectives on Organic Photovoltaics. *Polym. Rev.* **2010**, *50*, 411–419.
22. He, Z.; Zhong, C.; Su, S.; Xu, M.; Wu, H.; Cao, Y. Enhanced Power-Conversion Efficiency in Polymer Solar Cells Using an Inverted Device Structure. *Nat. Photon.* **2012**, *6*, 591–595.
23. Green, M. A.; Emery, K.; Hishikawa, Y.; Warta, W.; Dunlop, E. D. Solar Cell Efficiency Tables (Version 41). *Prog. Photovolt.: Res. Appl.* **2013**, *21*, 1–11.
24. You, J.; Dou, L.; Yoshimura, K.; Kato, T.; Ohya, K.; Moriarty, T.; Emery, K.; Chen, C.-C.; Gao, J.; Li, G.; *et al.* A Polymer Tandem Solar Cell with 10.6% Power Conversion Efficiency. *Nat. Commun.* **2013**, *4*, 1446.
25. Graetzel, M.; Janssen, R. A. J.; Mitzi, D. B.; Sargent, E. H. Materials Interface Engineering for Solution-Processed Photovoltaics. *Nature* **2012**, *488*, 304–312.
26. Wu, Y.; Zhang, G. Performance Enhancement of Hybrid Solar Cells through Chemical Vapor Annealing. *Nano Lett.* **2010**, *10*, 1628–1631.
27. Huynh, W. U.; Dittmer, J. J.; Teclemariam, N.; Milliron, D. J.; Alivisatos, A. P.; Barnham, K. W. J. Charge Transport in Hybrid Nanorod-Polymer Composite Photovoltaic Cells. *Phys. Rev. B* **2003**, *67*, 115326.
28. Li, Z.; Gao, F.; Greenham, N. C.; McNeill, C. R. Comparison of the Operation of Polymer/Fullerene, Polymer/Polymer, and Polymer/Nanocrystal Solar Cells: A Transient Photocurrent and Photovoltage Study. *Adv. Funct. Mater.* **2011**, *21*, 1419–1431.
29. Kramer, I. J.; Sargent, E. H. Colloidal Quantum Dot Photovoltaics: A Path Forward. *ACS Nano* **2011**, *5*, 8506–8514.
30. Sargent, E. H. Colloidal Quantum Dot Solar Cells. *Nat. Photon.* **2012**, *6*, 133–135.
31. Johnston, K. W.; Pattantyus-Abraham, A. G.; Clifford, J. P.; Myrskog, S. H.; Hoogland, S.; Shukla, H.; Klem, J. D.; Levina, L.; Sargent, E. H. Efficient Schottky-Quantum-Dot Photovoltaics: The Roles of Depletion, Drift, and Diffusion. *Appl. Phys. Lett.* **2008**, *92*, 122111.
32. Luther, J. M.; Gao, J.; Lloyd, M. T.; Semonin, O. E.; Beard, M. C.; Nozik, A. J. Stability Assessment on a 3% Bilayer Pbs/ZnO Quantum Dot Heterojunction Solar Cell. *Adv. Mater.* **2010**, *22*, 3704–3707.
33. Gao, J.; Luther, J. M.; Semonin, O. E.; Ellingson, R. J.; Nozik, A. J.; Beard, M. C. Quantum Dot Size Dependent J-V Characteristics in Heterojunction ZnO/PbS Quantum Dot Solar Cells. *Nano Lett.* **2011**, *11*, 1002–1008.
34. Klem, E. J. D.; Shukla, H.; Hinds, S.; MacNeil, D. D.; Levina, L.; Sargent, E. H. Impact of Dithiol Treatment and Air Annealing on the Conductivity, Mobility, and Hole Density in PbS Colloidal Quantum Dot Solids. *Appl. Phys. Lett.* **2008**, *92*, 212105.
35. Luther, J. M.; Law, M.; Song, Q.; Perkins, C. L.; Beard, M. C.; Nozik, A. J. Structural, Optical and Electrical Properties of Self-Assembled Films of PbSe Nanocrystals Treated with 1,2-Ethanedithiol. *ACS Nano* **2008**, *2*, 271–280.

36. Tang, J.; Kemp, K. W.; Hoogland, S.; Jeong, K. S.; Liu, H.; Levina, L.; Furukawa, M.; Wang, X. H.; Debnath, R.; Cha, D. K.; *et al*. Colloidal-Quantum-Dot Photovoltaics Using Atomic-Ligand Passivation. *Nat. Mater.* **2011**, *10*, 765–771.
37. Peng, Z. A.; Peng, X. G. Nearly Monodisperse and Shape-Controlled CdSe Nanocrystals via Alternative Routes: Nucleation and Growth. *J. Am. Chem. Soc.* **2002**, *124*, 3343–3353.
38. Barkhouse, D. A. R.; Pattantyus-Abraham, A. G.; Levina, L.; Sargent, E. H. Thiols Passivate Recombination Centers in Colloidal Quantum Dots Leading to Enhanced Photovoltaic Device Efficiency. *ACS Nano* **2008**, *2*, 2356–2362.
39. Liu, Y.; Gibbs, M.; Puthussery, J.; Gaik, S.; Ihly, R.; Hillhouse, H. W.; Law, M. Dependence of Carrier Mobility on Nanocrystal Size and Ligand Length in PbSe Nanocrystal Solids. *Nano Lett.* **2010**, *10*, 1960–1969.
40. Muhlbacher, D.; Scharber, M.; Morana, M.; Zhu, Z.; Waller, D.; Gaudiana, R.; Brabec, C. High Photovoltaic Performance of a Low-Bandgap Polymer. *Adv. Mater.* **2006**, *18*, 2884–2889.
41. Pivrikas, A.; Juska, G.; Mozer, A. J.; Scharber, M.; Arlauskas, K.; Sariciftci, N. S.; Stubb, H.; Osterbacka, R. Bimolecular Recombination Coefficient as a Sensitive Testing Parameter for Low-Mobility Solar-Cell Materials. *Phys. Rev. Lett.* **2005**, *94*, 176806.
42. Xue, J.; Rand, B. P.; Uchida, S.; Forrest, S. R. A Hybrid Planar-Mixed Molecular Heterojunction Photovoltaic Cell. *Adv. Mater.* **2005**, *17*, 66–71.
43. Li, G.; Shrotriya, V.; Huang, J. S.; Yao, Y.; Moriarty, T.; Emery, K.; Yang, Y. High-Efficiency Solution Processable Polymer Photovoltaic Cells by Self-Organization of Polymer Blends. *Nat. Mater.* **2005**, *4*, 864–868.
44. Owen, J. S.; Park, J.; Trudeau, P. E.; Alivisatos, A. P. Reaction Chemistry and Ligand Exchange at Cadmium-Selenide Nanocrystal Surfaces. *J. Am. Chem. Soc.* **2008**, *130*, 12279–12280.
45. von Holt, B.; Kudera, S.; Weiss, A.; Schrader, T. E.; Manna, L.; Parak, W. J.; Braun, M. Ligand Exchange of CdSe Nanocrystals Probed by Optical Spectroscopy in the Visible and Mid-IR. *J. Mater. Chem.* **2008**, *18*, 2728–2732.
46. Kopping, J. T.; Patten, T. E. Identification of Acidic Phosphorus-Containing Ligands Involved in the Surface Chemistry of CdSe Nanoparticles Prepared in Tri-*N*-octylphosphine Oxide Solvents. *J. Am. Chem. Soc.* **2008**, *130*, 5689–5698.
47. Morris-Cohen, A. J.; Donakowski, M. D.; Knowles, K. E.; Weiss, E. A. The Effect of a Common Purification Procedure on the Chemical Composition of the Surfaces of CdSe Quantum Dots Synthesized with Trioctylphosphine Oxide. *J. Phys. Chem. C* **2010**, *114*, 897–906.
48. Gomes, R.; Hassinen, A.; Szczygiel, A.; Zhao, Q. A.; Vantomme, A.; Martins, J. C.; Hens, Z. Binding of Phosphonic Acids to CdSe Quantum Dots: A Solution NMR Study *J. Phys. Chem. Lett.* **2011**, *2*, 145–152.
49. Wang, F.; Tang, R.; Kao, J. L. F.; Dingman, S. D.; Buhro, W. E. Spectroscopic Identification of Tri-*N*-octylphosphine Oxide (Topo) Impurities and Elucidation of Their Roles in Cadmium Selenide Quantum-Wire Growth. *J. Am. Chem. Soc.* **2009**, *131*, 4983–4994.
50. Hao, E.; Sun, H.; Zhou, Z.; Liu, J.; Yang, B.; Shen, J. Synthesis and Optical Properties of CdSe and CdSe/CdS Nanoparticles. *Chem. Mater.* **1999**, *11*, 3096–3102.
51. Yaacobi-Gross, N.; Soreni-Harari, M.; Zimin, M.; Kababya, S.; Schmidt, A.; Tessler, N. Molecular Control of Quantum-Dot Internal Electric Field and Its Application to CdSe-Based Solar Cells. *Nat. Mater.* **2011**, *10*, 974–979.
52. Yaacobi-Gross, N.; Garphunkin, N.; Solomeshch, O.; Vaneski, A.; Susha, A. S.; Rogach, A. L.; Tessler, N. Combining Ligand-Induced Quantum-Confined Stark Effect with Type II Heterojunction Bilayer Structure in CdTe and CdSe Nanocrystal-Based Solar Cells. *ACS Nano* **2012**, *6*, 3128–3133.
53. Xue, J.; Uchida, S.; Rand, B. P.; Forrest, S. R. Asymmetric Tandem Organic Photovoltaic Cells with Hybrid Planar-Mixed Molecular Heterojunctions. *Appl. Phys. Lett.* **2004**, *85*, 5757–5759.
54. Shrotriya, V.; Li, G.; Yao, Y.; Moriarty, T.; Emery, K.; Yang, Y. Accurate Measurement and Characterization of Organic Solar Cells. *Adv. Funct. Mater.* **2006**, *16*, 2016–2023.
55. Rand, B. P.; Xue, J.; Uchida, S.; Forrest, S. R. Mixed Donor-Acceptor Molecular Heterojunctions for Photovoltaic Applications. I. Material Properties. *J. Appl. Phys.* **2005**, *98*, 124902.